Group chase and escape in the presence of obstacles

J.R. Šćepanović [a], A. Karač [b], Z.M. Jakšić [a], Lj. Budinski-Petković [c], S.B. Vrhovac [a,*]

[a] *Scientific Computing Laboratory, Center for the Study of Complex Systems, Institute of Physics Belgrade, University of Belgrade, Pregrevica 118, Zemun 11080, Belgrade, Serbia*
[b] *Polytechnic faculty, University of Zenica, Bosnia and Herzegovina*
[c] *Faculty of Engineering, Trg D. Obradovića 6, Novi Sad 21000, Serbia*

HIGHLIGHTS

- Hunting in the presence of obstacles is studied.
- Dynamics of smart chasing and escape between two species is studied by MC simulations.
- Stretched exponential behavior excellently describes the capture dynamics.
- Characteristic time τ decreases with the initial density of targets as a power law.
- Characteristic timescale τ increases with the density of obstacles.

ARTICLE INFO

ABSTRACT

We study a stochastic lattice model describing the dynamics of a group chasing and escaping between two species in an environment that contains obstacles. The Monte Carlo simulations are carried out on a two-dimensional square lattice. Obstacles are represented by non-overlapping lattice shapes that are randomly placed on the lattice. The model includes smart pursuit (chasers to targets) and evasion (targets from chasers). Both species can affect their movement by visual perception within their finite sighting range σ.

We concentrate here on the role that density and shape of the obstacles plays in the time evolution of the number of targets, $N_T(t)$. Temporal evolution of the number of targets $N_T(t)$ is found to be stretched-exponential, of the form $N_T(t) = N_T(0) - \delta N_T(\infty)\left(1 - \exp[-(t/\tau)^\beta]\right)$, regardless of whether the obstacles are present or not. The characteristic timescale τ is found to decrease with the initial density of targets ρ_0^T according to a power-law, i.e., $\tau \propto (\rho_0^T)^{-\gamma}$. Furthermore, temporal dependences of the number of targets $N_T(t)$ are compared for various combinations of chasers and targets with different sighting ranges, $\sigma = 1,\ 2$, in order to analyze the relationship between the ability of species and the capture dynamics in the presence of obstacles.

© 2019 Elsevier B.V. All rights reserved.

1. Introduction

The collective motion of interacting living organisms such as bacteria colonies [1–3], amoeba [4–6], cells [7–9], insects [10,11], fish [12,13], birds [14,15], and humans [16–20] has drawn great attention of researchers from diverse fields in

---

* Corresponding author.
    E-mail address: vrhovac@ipb.ac.rs (S.B. Vrhovac).
    URL: http://www.ipb.ac.rs/~vrhovac/ (S.B. Vrhovac).

the past two decades [21]. Pursuit and evasion problems have a long and interesting history [22]. It is well known that collective motion of individuals with escape and pursuit behavior serve as a protection mechanisms against chasers. The goal for chaser (predator) and target (for example, prey) is to choose an efficient motion strategy that optimizes their respective chances of successful pursuit or evasion. At first, developing computational systems and techniques enabled one to deal with a two-particle system consisting of one chaser and one target, where there existed a challenging mathematical problem for obtaining analytical expressions [22]. Also, a class of pursuit-and-evasion problems involving a single evading prey that is being hunted by $N > 1$ predators has been modeled and analyzed [23–25]. In addition to these modeling efforts, extensive research has been devoted to developing multi-agent models that consider the role of multiple predators and/or preys [26–35].

Kamimura and Ohira [26] have introduced a lattice model to analyze the group spatial chase and escape phenomena. The model assumes that chasers and targets are initially placed randomly on the square lattice as pointlike particles. Both species perform independent nearest-neighbor random walks on a lattice following simple dynamical rules, increasing or decreasing the distance from the nearest particle of the opposite group. Chasers start a direct chase whenever a target appears within their sighting range. Targets try to evade capture by making a distance of one lattice spacing in a direction away from the nearest chaser. Target is caught upon the first encounter with a chaser. In their model, although each chaser independently moves in order to catch one of the nearest targets, some groups of chasers are simultaneously formed. In the simulation, the chasers form flocks and seem to cooperate to catch the flocks of targets [24,26,33,34,36]. In the basic version of the model, chasers can sense the positions of the targets at an arbitrary distance. The authors have considered several extensions to this simplest version of the model, including the search range of chasers and targets, and introduction of a term designed to account for random fluctuations that are usually present in real systems. Despite its simplicity, the model is able to reproduce a lot of interesting behaviors [27].

Based on a concept proposed by Kamimura and Ohira [26] we built up a bio-inspired realistic agent-based approach to model collective chasing and escaping in a discrete space and time with periodic boundary conditions for the case when the lattice is initially covered with obstacles at various concentrations. The depositing objects (obstacles) are formed by a small number of lattice steps on the square lattice. Spatial distribution of the obstacles on the lattice is created using the random sequential adsorption (RSA) method [37,38]. The dominant effect in RSA is the blocking of the available surface area. When the surface is saturated by the adsorbed objects so that no further objects can be placed, the system reaches the jamming limit ρ_J. Thus, an element of stochasticity of environment, which is present in any natural system, is incorporated into the model. It must be emphasized that birth and death processes [39,40] are not considered here, so the results obtained apply only on the time scales short compared to the typical lifetime of single organisms. The role of multiple predators and preys has also been studied by using an off-lattice models [41,42], based on the modeling of the self-propelled organisms by Vicsek et al. and including the chase-escape mechanisms through simple intergroup pairwise interactions [43]. In such models, an analysis of the impact of geometrically complex boundary conditions, such as obstacles, would require taking into account a hard core repulsion term in the interaction. However, the lattice-based models allow easier handling of objects (obstacles) of various shapes and sizes.

For the real life systems, simulation resembles to two animal species fighting for the survival. Obstacles may be trees, rocks, or anything that is big enough for the evader and pursuer to become "invisible" for the other. The chasers and evaders can also be human beings, but with different roles, like police officers and robbers, where buildings, grocery stores and similar objects can be viewed as obstacles.

We study the survival of N_0^T targets (for example, prey) that is captured by N_0^C chasers (predators) in the presence of static obstacles. We have kept the rules governing the dynamics of the processes at the individual level as simple as possible to focus entirely on the effects of obstacles. Each species has its specific sighting range σ in which it can see the other species. In [26], for each target, the distance to each chaser is calculated as the Euclidean distance. Unlike the Kamimura and Ohira model [26], distances as well as sighting ranges in the present study are measured by a L^1 ("Manhattan") metric. Manhattan distance between sites P_1 and P_2 on a square lattice is equal to the length of all paths connecting P_1 and P_2 along horizontal and vertical segments, without ever going back. Therefore, Manhattan metric more correctly than Euclidean's determines the length of the path between two sites in the lattice-based models. In our model, there are two types of chasers and targets and each of them has its own sighting range σ, which describes their skills at chasing and escaping, respectively. In reality, chasers search for targets in their vicinities. Similarly, targets can recognize the existence of nearby chasers. Therefore, analysis of the capture dynamics in the present study is limited to species with two different sighting ranges, i.e., $\sigma = 1$, 2. If the value of σ equals zero, the movement is equivalent to the random walkers [26,28,40,44]. It has been confirmed that the idea of animals using blind search strategies does not seem to be usable since it neglects the role of animals' smartness and experience in guiding them [45]. We investigate the role that the density of obstacles plays in the time evolution of the number of targets, $N_T(t)$. A detailed analysis of the contribution to the capture dynamics coming from the size and the shape of obstacles is carried out. Furthermore, temporal dependences of the number of targets $N_T(t)$ in the presence of obstacles are compared for various combinations of chasers and targets with different chasing and avoidance skills in order to analyze the relationship between the ability of species and the capture dynamics. In particular, we try to find a universal functional type that describes the decrease in the number of targets $N_T(t)$ in the best way.

We organized the paper as follows. Section 2 describes the details of the model and simulations. In Section 3 results of numerical simulation are presented and discussed. Finally, Section 4 contains some additional comments and final remarks.

2. Definition of the model and the simulation method

The environment where two interacting species coexist is represented by the two-dimensional square lattice of linear size L with periodic boundary conditions. In our model the lattice is initially occupied by obstacles of various shapes and sizes at the effective density ρ_0. This density is defined as a fraction of sites of the lattice that are occupied by the obstacles. Linear obstacles are k-mers of length $\ell = k - 1 = 0, 1, \ldots, 6$, shown in Table 1 as objects (A_1)–(A_7). Extended shapes that we have used as obstacles are the crosses of two different sizes, shown in Table 2 as objects (C_1) and (C_2).

Obstacles cannot overlap and their spatial distribution at density ρ_0 is generated using the random sequential adsorption (RSA) method [37,38]. In the case of mixtures of obstacles, at each deposition attempt, one of the objects that makes the mixture is selected at random and deposition of the selected object is tried in a randomly chosen lattice site. In this way we are able to prepare the environment in disordered initial state with a statistically reproducible density ρ_0 of obstacles. To initialize the model, N_0^C chasers and N_0^T targets are randomly distributed as monomers in the lattice. Each site can be either empty or occupied by one particle: by a chaser or escapee (target) or by a particle that belongs to an obstacle.

After placing the chasers and the targets up to the chosen densities $\rho_0^C = N_0^C/L^2$ and $\rho_0^T = N_0^T/L^2$, we switch the species deposition events off and initiate a random diffusive dynamics in the system. At this stage, apart from the hard core interaction between the species, and between the species and the obstacles, there are simple rules governing the dynamic processes at the individual level. Movement within the lattice and the population dynamics are modeled as discrete time processes. At each Monte Carlo step a lattice site is selected at random. If the selected site is unoccupied or occupied by an obstacle, the configuration remains unchanged and a new site is selected at random. If the selected site is occupied by a chaser or an escapee, each species follow the hopping rules described below.

Chaser has a certain pursuit region within which it can locate targets; simultaneously, target has an escape zone inside which it can detect chasers. In other words, each species has its specific sighting range σ in which it can see the other species. By definition, the metric is L^1, so e.g. the site (x, y) is at distance $|x| + |y|$ from the origin, with lattice spacing equal to unity. Two types of chasers and targets are used in our model depending on the sighting range σ: Chasers-I and Targets-I have sighting range $\sigma = 1$, while for Chasers-II and Targets-II, $\sigma = 2$.

Suppose that Chaser-I is placed in a randomly selected site of the lattice. If the first neighbors of the selected site are entirely occupied with obstacles and chasers, the chosen chaser stays at its original position. Then, the time t is updated, $t \rightarrow t + 1/L^2$ and the process continues by choosing a new lattice site at random. Suppose that some of the first neighbors of the selected site are occupied with targets. Then we randomly select a target among them, remove the selected target from the grid, and move the chosen chaser to this empty place. However, if the first neighbors of the chosen chaser are not occupied with targets, the chaser executes a jump as long as there is at least one empty nearest neighbor site. In this case, the chaser is moved to the randomly selected empty adjacent site.

Now, suppose that Target-I is placed in a randomly selected site of the lattice. If there are no empty nearest neighbors of the selected site, the chosen target does not change its position, and the time increases by $1/L^2$. If the selected site has empty adjacent sites, the chosen target moves into one of them randomly.

In our model we introduce chasers and targets with different chasing and avoidance skills, respectively, depending on the sighting range σ. Accordingly, decision for every step both of the Chaser-II and Target-II depends on the species that are found at the places of second neighbors. Algorithms for movement of species I and II are different only in the method of selection of the empty neighboring sites for a jump. Species I randomly chooses an empty nearest neighbor site for a jump. However, Chaser-II moves to the empty adjacent site that is surrounded by the highest number of targets, $n_T^{(max)}$, as its first neighbors (see, Fig. 1(a)). On the contrary, Target-II jumps to the empty nearest neighbor site that is surrounded by the lowest number of chasers, $n_C^{(min)}$, as its first neighbors (see, Fig. 1(b)). If two or more empty nearest neighbor sites correspond to the same highest/lowest number of targets $n_T^{(max)}$/chasers $n_C^{(min)}$, one of them is selected at random. It must be emphasized that Target-II moves to the selected site only if $n_C^{(min)}$ is less than or equal to the number of chasers surrounding it in its original position. In both cases when the sighting range σ is one or two, pursuer and evader can move only to a neighboring site. Neither chasers nor evaders can see through the obstacles and they make their decision about the movement without the knowledge of the situation behind the obstacle.

The time t is counted by the number of attempts to select a lattice site and scaled by the total number of lattice sites $N = L^2$. Since in one Monte Carlo time step each lattice site is randomly checked once on the average, it can be considered that all chasers and targets are active at all times and that none of the species have a priority in the number of attempts to make a move. The simulation data are averaged over 100 independent runs for each coverage of obstacles and each initial chasers and targets concentrations.

The simulations have been performed for a wide range of obstacle densities, $\rho_0 < 0.45$, below the corresponding percolation thresholds [46,47]. Considering the underlying percolation problem on the lattice, a geometric transition occurs at the percolation threshold p_c^*, above which the void space falls completely apart into finite clusters. As density of obstacles is increased above a certain critical value p_c^*, the initial large cluster of empty lattice space breaks into tiny non-communicating components and connectivity between both sides of the lattice disappears. In this case, spatially separated groups of chasers and targets can be formed on the lattice during the initialization process. Such artificial situations will not be considered in this paper.
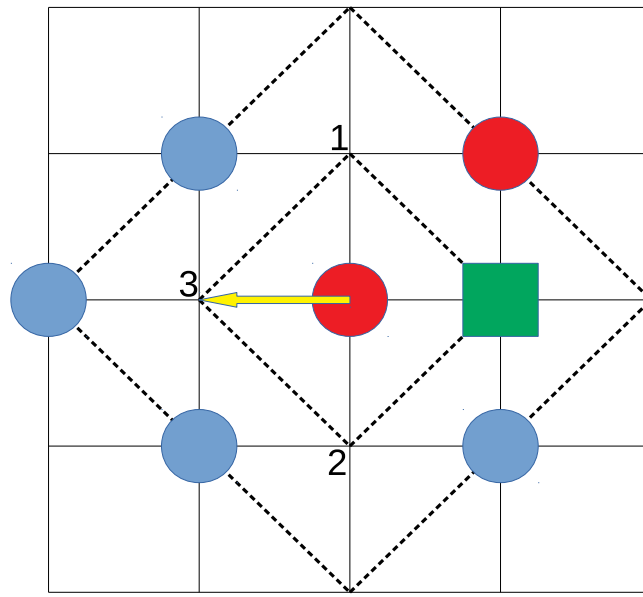
(a)
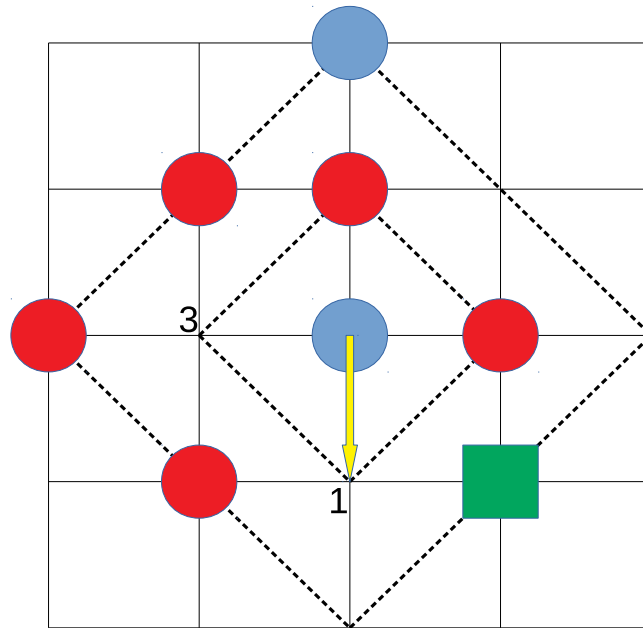
(b)

Fig. 1. Hopping rules for (a) chasers and (b) targets. Diamonds represent their respective sighting ranges, $\sigma = 1, 2$. The green squares show the obstacles. Chasers (red circles) look for the nearest target and move to one of the nearest sites in order to catch the target. Targets (blue circles) try to escape from the nearest chaser. When a target is in a site nearest to a chaser, the chaser catches the target by hopping to the site, and then the target is removed from the system. Panel (a): Yellow arrow from the chaser to the adjacent site indicates that the Chaser-II hops to the empty site that is surrounded by the highest number of targets ($n_T^{(max)} = 3$). Chaser-I has three choices. Panel (b): Yellow arrow from the target to the adjacent site indicates that Target-II hops to the empty site that is surrounded by the lowest number of chasers ($n_C^{(min)} = 1$). Target-I has two choices. Values of the number of the nearest targets and chasers are given for the empty adjacent sites.
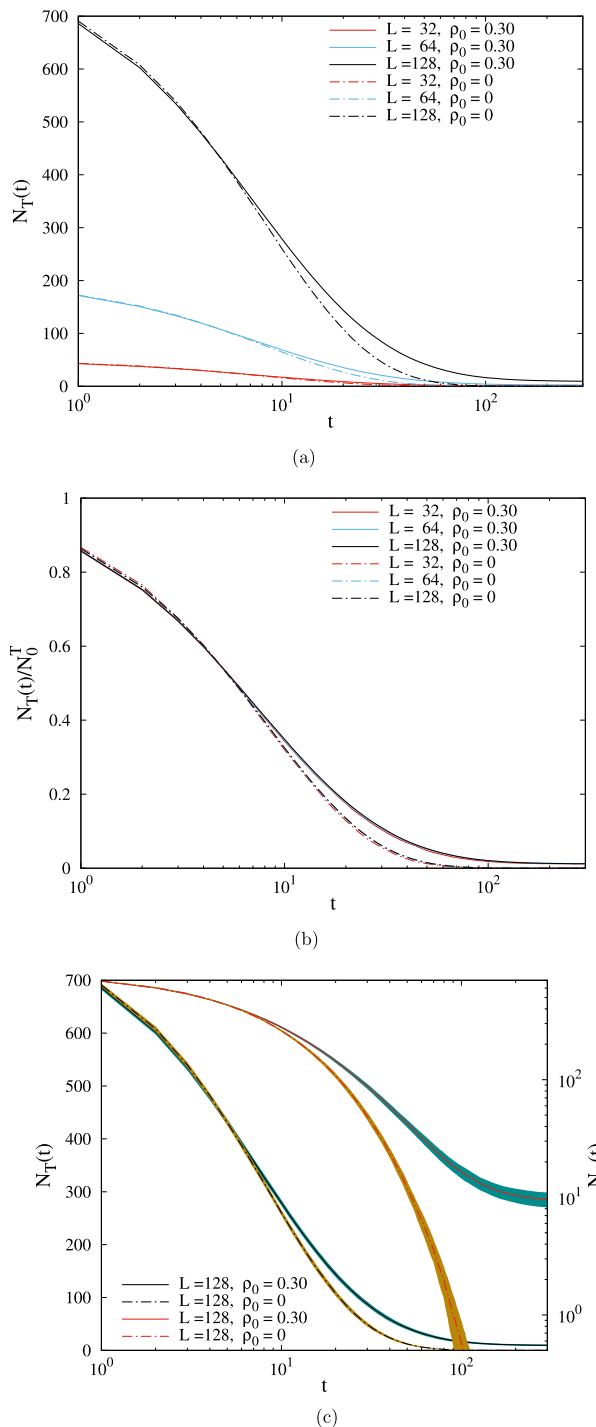
(a)

(b)

(c)

Fig. 2. Time dependences of the number of targets $N_T(t)$ (panel (a)) and of the normalized number of targets $N_T(t)/N_0^T$ (panel (b)) on the lattices of size $L = 32$, 64, and 128, as indicated in legend. The full curves represent the results obtained when obstacles are the binary mixtures of trimers (A_3) and crosses (C_1) of density $\rho_0 = 0.30$ (see, Tables 1 and 2). The dashed curves represent the results obtained in the absence of obstacles. Panel (c): Shown here are the temporal dependences of the number of targets $N_T(t)$ on the lattice of size $L = 128$, obtained for the same conditions as in panel (a) (see legend). The black (red) lines are plotted against the left-hand (right-hand) axis. The shaded region represents the standard deviation. Results shown in panels (a), (b), and (c) are obtained for the same initial densities $\rho_0^C = 0.0439$ and $\rho_0^T = 0.0488$, for all lattices. Initial values for the number of chasers/targets are $N_0^C/N_0^T = 45/50, 180/200, 720/800$ for $L = 32, 64, 128$, respectively.

3. Results and discussion

While the number of chasers, $N_C(t)$, remains constant N_0^C, the number of targets, $N_T(t)$, monotonically decreases along with the catches. Here we focus on the model that includes species with sighting range $\sigma = 2$ (Chasers-II + Target-II), and study the effects of obstacles on the time evolution of the number of targets, $N_T(t)$. In addition, we will compare the results for all four combinations of previously defined species I and II, as shown in Table 3.

In our model, lattice size L is an arbitrary parameter. In Fig. 2(a) we show the temporal dependence of the number of targets $N_T(t)$ on the lattices of size $L = 32$, 64, and 128, when obstacles are the binary mixtures of trimers (A_3) and crosses (C_1) of density $\rho_0 = 0.30$ (see, Tables 1 and 2). For comparison, we also plot the temporal dependences of the number of targets $N_T(t)$ in the absence of obstacles for these three lattices. It is important to note that the initial densities of chasers ρ_0^C and targets ρ_0^T have not changed with the lattice size L. Numerical results for $N_T(t)$ in Fig. 2(a) are given for the initial densities $\rho_0^C = 0.0439$ and $\rho_0^T = 0.0488$, with the same ratio $\rho_0^C/\rho_0^T = N_0^C/N_0^T = 0.9$ for all the lattices. In Fig. 2(b), the values of the normalized number of targets $N_T(t)/N_0^T$ versus the time t are presented for the simulation results shown in Fig. 2(a). It is evident that for the given density of the obstacles ρ_0, the time evolution of the normalized number of targets $N_T(t)/N_0^T$ does not depend on the lattice size L. However, for the lattice of fixed size L, time evolution of $N_T(t)/N_0^T$ depends on the initial number of chasers N_0^C and targets N_0^T. We shall return to this point later on in connection with the relationship between the densities of species and dynamics of the model.

In Fig. 2(c) we show the temporal dependence of the number of targets $N_T(t)$ on the lattice of size $L = 128$ obtained for the same conditions as in Fig. 2(a). The shaded strips in Fig. 2(c) indicate an interval of one standard deviation above and below the estimated mean value. In addition, the double logarithmic plots of the same results are also shown in the same panel. In this way, a better insight into the values of the standard deviation during the entire process is enabled. Standard deviations from the average value of $N_T(t)$ are of the order $\pm 1\%$ throughout the whole process of interest. In very late times, when the number of targets disappears, the standard deviation is less than 10%. As it can be seen, the statistical error bars slightly exceed the line thickness.

It must be stressed that all simulations have been performed in the conditions of sufficiently low densities of agents. In this way, we have tried to avoid the effects of the self volume [34,48,49]. In reality, chasers and targets are impenetrable bodies. For example, in an abundant population of prey, the prey species may obstruct each other while trying to escape. Moreover, at sufficiently large densities of targets, target can be temporarily trapped in "cages" formed by their neighbors of the *same species*. Then the motion of target is restricted by a shell of nearest neighbors, and its movement is influenced by the effect of trapping. However, in our model, agents can be temporarily caged by a dense network of obstacles. In order to make the analysis of the results simpler, it is necessary that these two effects are not present in simulations at the same time. Consequently, all simulations are carried out in the conditions of sufficiently low densities of agents.

In the absence of obstacles, simulations are carried out until all targets have been caught by chasers, i.e. $N_T(t) = 0$. However, in the presence of obstacles, there may be targets that cannot be eliminated by the chasers. Such targets are located within clusters of empty sites ("cages") in which chasers have not been deposited during the initialization process. The number of inaccessible targets increases with the density of obstacles ρ_0. Fig. 3 shows two typical snapshot configurations obtained in the case of the binary mixture of obstacles (trimers (A_3) and crosses (C_1)) of density $\rho_0 = 0.30$. The snapshots are taken at the beginning of the process ($t = 1$), and after a long enough time ($t = 300$) when only a few targets ($N_T(300) = 6$) are left in the "cages" formed by obstacles.

Now, we present and discuss the numerical results regarding the time evolution of the number of targets $N_T(t)$ in the absence of obstacles, for several initial densities of chasers ρ_0^C and targets ρ_0^T on the lattice of the fixed size $L = 128$. The initial numbers of species (N_0^C, N_0^T) were chosen as (20, 25), (40, 50), (80, 100), (160, 200), (320, 400), and (640, 800), so that we have the same ratio $N_0^C/N_0^T = 0.8$ in all simulation runs. Temporal evolution of the normalized number of targets $N_T(t)/N_0^T$ for various initial densities $\rho_0^C = N_0^C/L^2$ and $\rho_0^T = N_0^T/L^2$ (provided that $\rho_0^C/\rho_0^T = 0.8$) are presented in Fig. 4. We observe that the decrease of $N_T(t)/N_0^T$ with time gets drastically slower when the initial densities ρ_0^C and ρ_0^T decrease. Analyzing the curves in Fig. 4 we find that the decrease of $N_T(t)/N_0^T$ is slower than exponential in time. In addition, the curves for different values of the initial density of species are very similar in form. In order to provide the best analytical approximation for the temporal behavior of the number of targets $N_T(t)$, we have probed a wide set of phenomenological fitting functions for relaxation processes in many complex disordered systems [50]. The best agreement with our simulation data was obtained by the Kohlrausch–Williams–Watts (KWW) or stretched exponential function. The fitting function we have used is of the form:

$$\frac{N_T(t)}{N_0^T} = 1 + \left(\frac{N_T(\infty)}{N_0^T} - 1\right)\left(1 - \exp\left[-\left(\frac{t}{\tau}\right)^\beta\right]\right), \tag{1}$$

where β is the parameter measuring the deviation from the single exponential form ($0 < \beta \leq 1$) and τ is the characteristic time. Fits of this stretched exponential form to the simulation data are shown as dashed lines in Fig. 4. Since the asymptotic number of targets $N_T(t) \to N_T(\infty)$, $t \gg \tau$, in the absence of the obstacles is equal to zero for all initial densities of species, the characteristic time τ can be defined as the time it takes for the simulation curves of $N_T(t)/N_0^T$ to fall to the level of $1/e$, i.e., $N_T(\tau)/N_0^T = 1/e$. In the absence of obstacles, the fitting parameter τ is given in Fig. 5 as a function of the initial density of targets ρ_0^T, for two values of the ratio $N_0^C/N_0^T = 0.8, 1.0$. In numerical simulations with the ratio $N_0^C/N_0^T = 1.0$, the

Fig. 3. Typical configurations of chasers (red dots) and targets (blue dots) at lattice of size $L = 64$ in the case of the binary mixture of obstacles (trimers (A_3) and crosses (C_1)) of density $\rho_0 = 0.30$. The snapshots are taken at the beginning of the process ($t = 1$, panel (a)), and after long enough times ($t = 300$, panel (b)) when only six targets are left on the lattice. Five cages with the remaining targets are marked on the panel (b) with thin blue lines. Initial number of chasers/targets is $N_0^C/N_0^T = 180/200$.

initial numbers of species were chosen to be $N_0^C = N_0^T = 25$, 50, 100, 200, 400, and 800. It is obvious that the parameter τ seems to be a simple power law of the initial density of targets ρ_0^T:
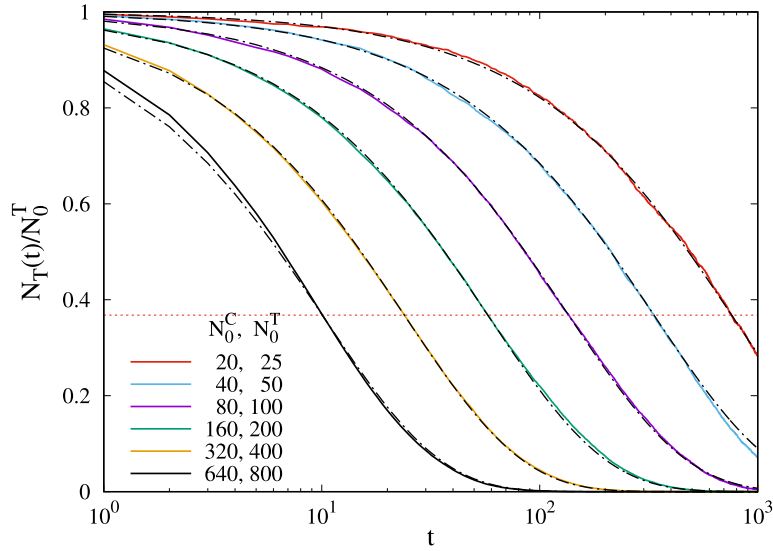
Fig. 4. Temporal evolution of the normalized number of targets $N_T(t)/N_0^T$ obtained in the absence of obstacles on the lattice of the size $L = 128$, and for various initial numbers of species (N_0^C, N_0^T), as indicated in the legend. The dashed curves are the stretched exponential fits of Eq. (1), with the parameter τ given in Fig. 5 and $\beta = 0.802$. Here, the ratio $N_0^C/N_0^T = \rho_0^C/\rho_0^T = 0.8$ is the same in all simulation runs. The horizontal dashed line indicates the $1/e$ value.
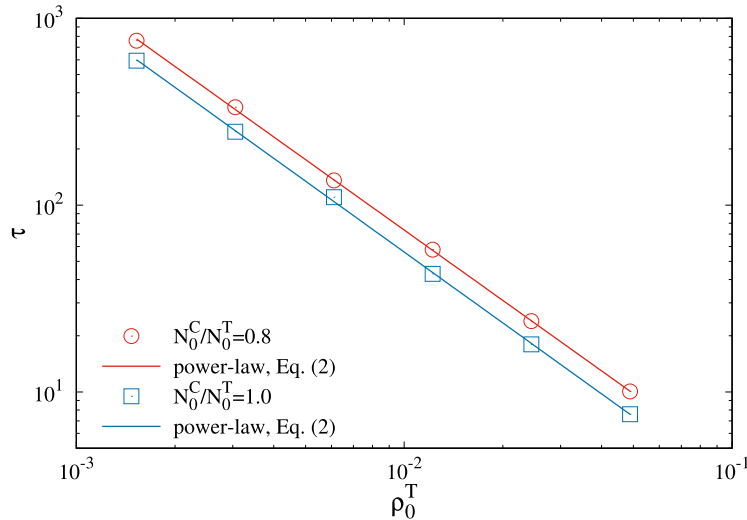

Fig. 5. Fitting parameter τ of the fit (1), as a function of the initial density of targets ρ_0^T in the case of the absence of obstacles, for two values of the initial ratio of chasers to targets $N_0^C/N_0^T = 0.8$, 1.0. The straight lines are the fits using Eq. (2). Dependence of τ on ρ_0^T seems to be well described by the simple power law (2). The values of fitting parameters are $A = 0.230$, $\gamma = 1.252$, $\beta = 0.802$ for $N_0^C/N_0^T = 0.8$; for $N_0^C/N_0^T = 1.0$, the fitting parameters are $A = 0.169$, $\gamma = 1.261$, and $\beta = 0.805$.

$$\tau = A \left(\rho_0^T\right)^{-\gamma}. \tag{2}$$

Exponent γ is approximately equal to $\gamma = 1.256 \pm 0.006$ for all examined ratios N_0^C/N_0^T. On the other hand, the stretching exponent β has the values below one, which confirms the nonexponential functional dependence of $N_T(t)/N_0^T$. Furthermore, for the fixed value of ratio N_0^C/N_0^T the exponent β is rather weakly dependent on the initial density of targets ρ_0^T. This provides the collapse of $N_T(t)/N_0^T$ vs. t curves onto a single curve when the time is scaled as t/τ. Fig. 6 shows the time-density superposition of the $N_T(t)/N_0^T$ curves in the case of the ratio $N_0^C/N_0^T = 0.8$, for all initial densities of species investigated. This figure clearly demonstrates the existence of a single universal master function.
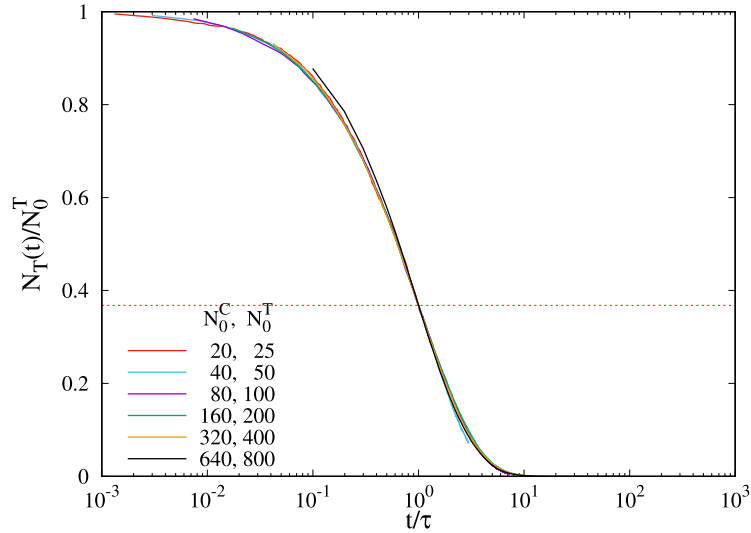
Fig. 6. Normalized number of targets $N_T(t)/N_0^T$ obtained in the absence of obstacles and rescaled to t/τ, for various initial numbers of species (N_0^C, N_0^T), as indicated in the legend. Here, the ratio $N_0^C/N_0^T = \rho_0^C/\rho_0^T = 0.8$ is the same in all simulation runs. The horizontal dashed line indicates the $1/e$ value.
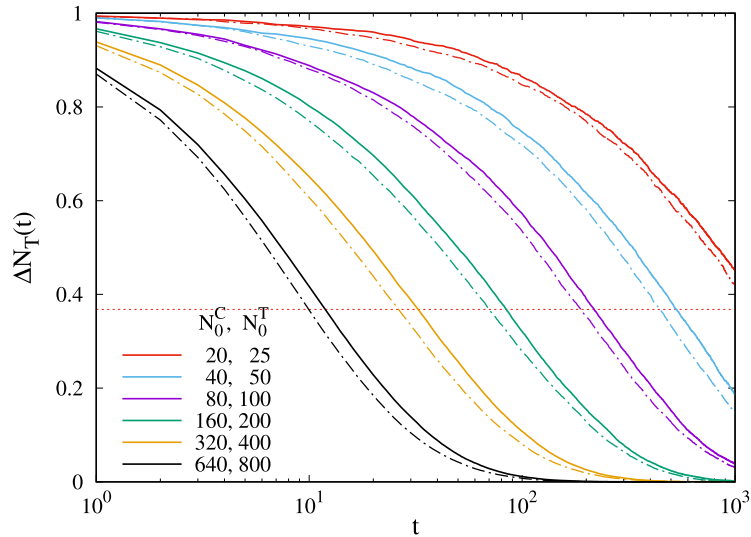

Fig. 7. Temporal evolution of the normalized deviation $\Delta N_T(t)$ (Eq. (3)) of the number of targets $N_T(t)$ obtained in the presence of obstacles (A_1) (solid lines) and (C_1) (dashed lines) on the lattice of size $L = 128$, and for various initial numbers of species (N_0^C, N_0^T), as indicated in the legend. Here, the ratio $N_0^C/N_0^T = \rho_0^C/\rho_0^T = 0.8$ is the same in all simulation runs. The horizontal dashed line indicates the $1/e$ value.

In the following, we analyze the time evolution of the number of targets $N_T(t)$ in the presence of obstacles, for various initial densities of chasers ρ_0^C and targets ρ_0^T on the lattice of the fixed size, $L = 128$. In order to gain a better insight into the effect of obstacles on the capture dynamics, simulations are performed both for point-like obstacles (A_1) and for obstacles of cruciform shape (C_1) covering five lattice sites (see, Tables 1 and 2). Furthermore, the results are obtained for the various values of density of the obstacles, $\rho_0 = 0.15, 0.20, 0.25,$ and 0.30. Let us first focus our attention on the representative results given in Fig. 7 for the case of density $\rho_0 = 0.25$. Fig. 7 shows the time evolution of the normalized deviation $\Delta N_T(t)$ of the number of targets $N_T(t)$ from the asymptotic value $N_T(\infty)$ for various initial densities ρ_0^C and ρ_0^T, provided that $N_0^C/N_0^T = \rho_0^C/\rho_0^T = 0.8$. The quantity $\Delta N_T(t)$ is defined as

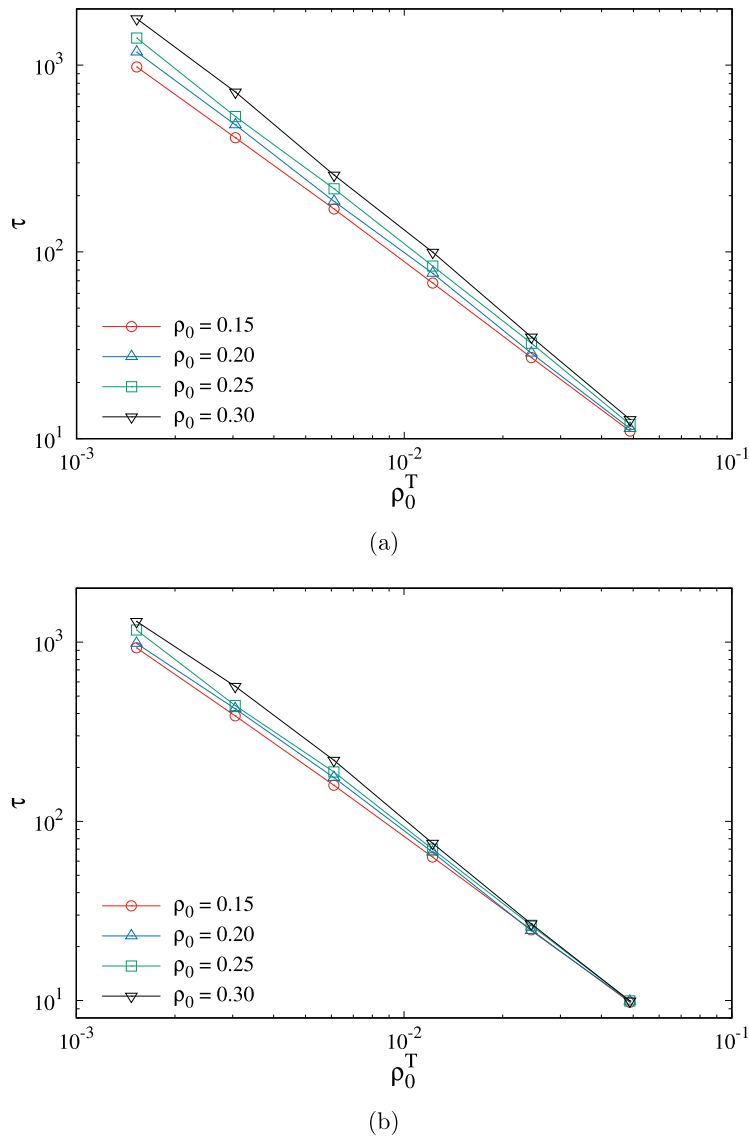$$\Delta N_T(t) = \frac{N_T(t) - N_T(\infty)}{N_0^T - N_T(\infty)}. \tag{3}$$

Fig. 8. Fitting parameter τ of the fit (1), as a function of the initial density of targets ρ_0^T in the case of the presence of (a) obstacles (A_1), and (b) obstacles (C_1). The curves in each graph correspond to various values of the density of obstacles $\rho_0 = 0.15, 0.20, 0.25, 0.30$, as indicated in the legend. All the results are for $N_0^C/N_0^T = 0.8$.

As in the case of the absence of obstacles, we observe that the decrease of $N_T(t)/N_0^T$ with time gets slower with the decrease in the initial densities ρ_0^C and ρ_0^T. Comparing the results from Fig. 7 for different obstacles at the same density $\rho_0 = 0.25$, one can see that the number of targets $N_T(t)$ in the case of point-like obstacles (A_1) decreases more slowly in time than for the case of obstacles of cruciform shape (C_1). This change in the capture dynamics is the result of a different structure of empty space that is formed after the deposition of obstacles of different size up to the chosen coverage fraction ρ_0. Actually, the mesh structure of the open spaces look very different for the adsorbing point-like obstacles (A_1) in comparison with the extended obstacles (C_1) [38,51]. Deposition of the extended obstacles (C_1) is characterized by domains of large islands of unoccupied sites. On the other hand, small obstacles such as monomers (A_1) cover the surface more uniformly, so that the empty space on the lattice is broken into small areas. Such a different free space view is the cause of the enhanced mobility of species in the case of cruciform shapes (C_1) as compared to those in the case of point-like shapes (A_1), resulting in a faster decrease of the number of targets $N_T(t)$ in the former case.

It must be stressed that the stretched-exponential fit (Eq. (1)) also accurately describes the temporal dependence of the number of targets $N_T(t)$ in the presence of obstacles (not shown here). Dependences of the nonlinear fitting parameter τ on the initial density of targets ρ_0^T are shown in Fig. 8 on a double logarithmic scale for various densities of obstacles (A_1) and (C_1), $\rho_0 = 0.15 - 0.30$. For all examined densities and obstacle shapes these plots are nearly straight lines, indicating
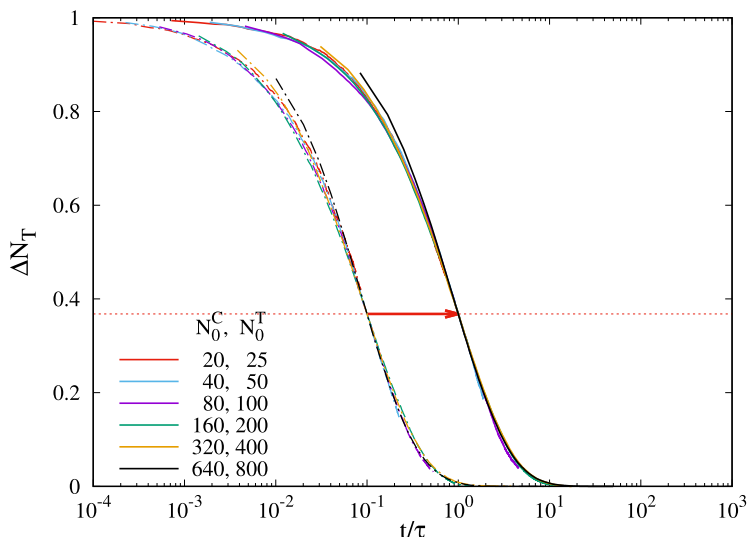
Fig. 9. Normalized deviation $\Delta N_T(t)$ (Eq. (3)) of the number of targets $N_T(t)$ obtained in the presence of obstacles (A_1) (solid lines) and (C_1) (dashed lines) and rescaled to t/τ, for various initial numbers of species (N_0^C, N_0^T), as indicated in the legend. For clarity, the data for obstacle (C_1) are shifted to the left ($t \rightarrow t/10$). Here, the lattice size is $L = 128$, density $\rho_0 = 0.25$, and the initial ratio of chasers to targets $N_0^C/N_0^T = \rho_0^C/\rho_0^T = 0.8$ are the same in all simulation runs. The horizontal dashed line indicates the $1/e$ value.
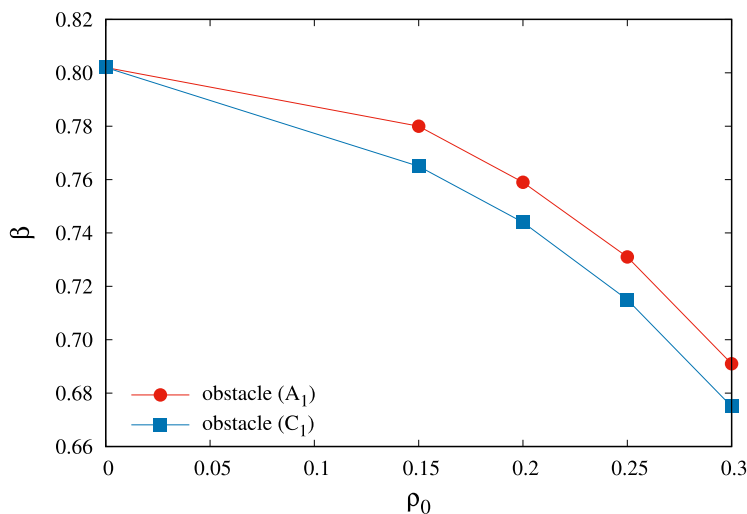

Fig. 10. Parameter β of the fit (1) *vs.* the density ρ_0 of the obstacles. Circles and squares correspond to obstacles (A_1) and (C_1) in Tables 1 and 2, respectively. Other parameters: $L = 128$, $N_0^C/N_0^T = \rho_0^C/\rho_0^T = 0.8$.

that the fitting parameter τ is a simple power-law of the initial density of targets ρ_0^T (see Eq. (2)). As in the case of the absence of obstacles, we observe that the dynamical behavior of our model is severely slowed down with the decrease of the initial densities ρ_0^C and ρ_0^T. In addition, the characteristic time τ is found to increase with the density of obstacles ρ_0. As one can see from Figs. 8(a) and 8(b), the increase of τ with ρ_0 is more pronounced for the lower initial densities of targets. Indeed, the efficiency of chasing becomes very high at larger densities of targets and weakly dependent on the presence of obstacles, due to the smaller mean distance between chasers and targets. Then the chasers quickly and efficiently find the neighboring targets, regardless of whether there are obstacles or not. However, for the lower initial concentration of targets the presence of obstacles noticeably slows down the dynamics of the system. We notice, the lower is the concentration of the targets, the longer is the mean distance that a chaser crosses to find a target and catch it. Along the longer path, chaser will interact with a larger number of obstacles. Therefore, obstacles more effectively suppress the chasing for lower densities of targets. Also, at sufficiently low densities of targets, obstruction of chasing is more pronounced at the higher densities of the obstacles.
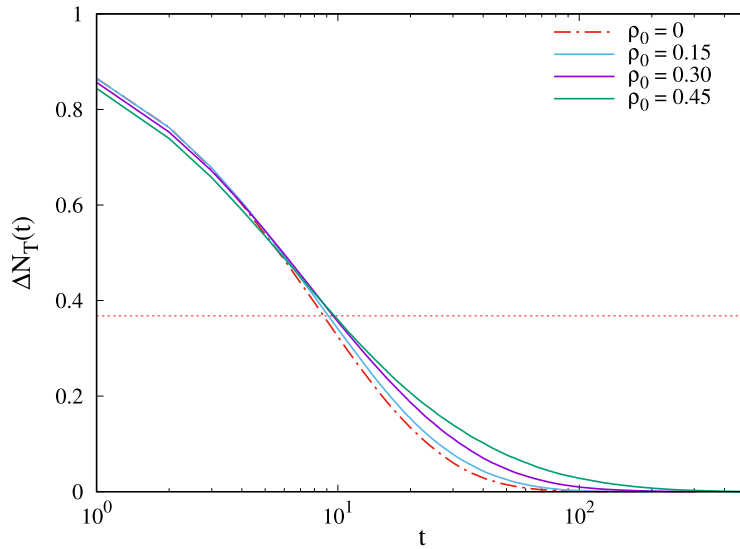
Fig. 11. Temporal evolution of the normalized deviation $\Delta N_T(t)$ (Eq. (3)) of the number of targets $N_T(t)$ obtained in the presence of obstacles (A_3) (solid lines) for various densities ρ_0, as indicated in the legend. The dashed line represents the temporal behavior of $\Delta N_T(t)$ in the absence of obstacles. Other parameters: $L = 128$, $N_0^C/N_0^T = 720/800 = 0.9$.

Fig. 12. Temporal evolution of the normalized deviation $\Delta N_T(t)$ (Eq. (3)) of the number of targets $N_T(t)$ obtained in the presence of obstacles ($A_1, A_2, \ldots, A_7$) of density $\rho_0 = 0.30$ (solid lines). The dashed line represents the temporal behavior of $\Delta N_T(t)$ in the absence of obstacles. Other parameters: $L = 128$, $N_0^C/N_0^T = 720/800 = 0.9$.
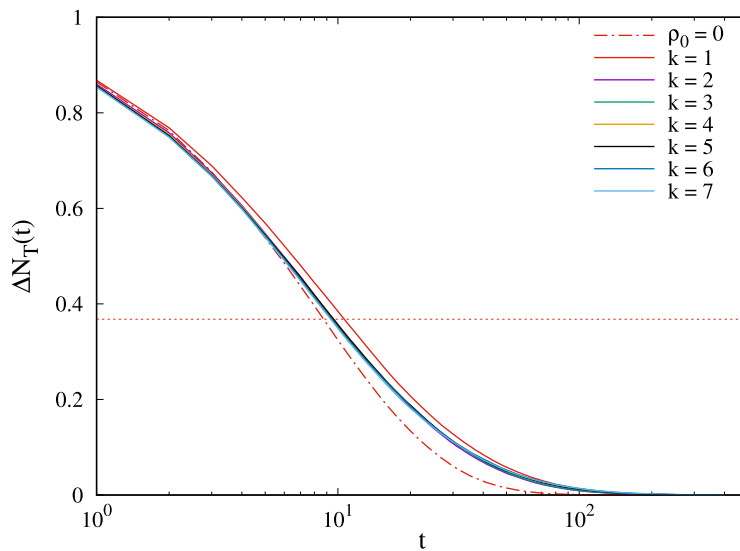
Fig. 9 illustrates that when the normalized deviations $\Delta N_T(t)$ (see, Eq. (3)) presented in Fig. 7 are plotted as a function of t/τ, the data for the all initial numbers of targets, $N_0^T = 25, 50, 100, 200, 400$ and 800, collapse onto a single curve. We note that different choices of obstacles give qualitatively similar results. This superposition of ΔN_T vs. t/τ curves is a consequence of the fact that for the fixed values of ratio N_0^C/N_0^T and density of obstacles ρ_0, the fitting parameter β is rather weakly dependent on the initial density of targets ρ_0^T. However, the stretching exponent β depends on the density ρ_0 of the obstacles. Fig. 10 shows dependence of parameter β on density ρ_0 for the two types of obstacles ((A_1) and (C_1)). Parameter β measures the rate of the chasing process on the time scale determined by the parameter τ. Consequently, in the late stage of the chasing process the decay rate of the number of targets $N_T(t)$ for the point-like obstacles (A_1) is higher than for the extended obstacles (C_1).

Now we consider in more details the influence of the length ℓ and density ρ_0 of the linear segments that make the obstacles on the temporal behavior of the number of targets $N_T(t)$. The simulations have been performed for linear segments (k-mers) of lengths $\ell = k - 1$, $k = 1, 2, \ldots, 7$ (see, Table 1), and for a wide range of obstacle densities,
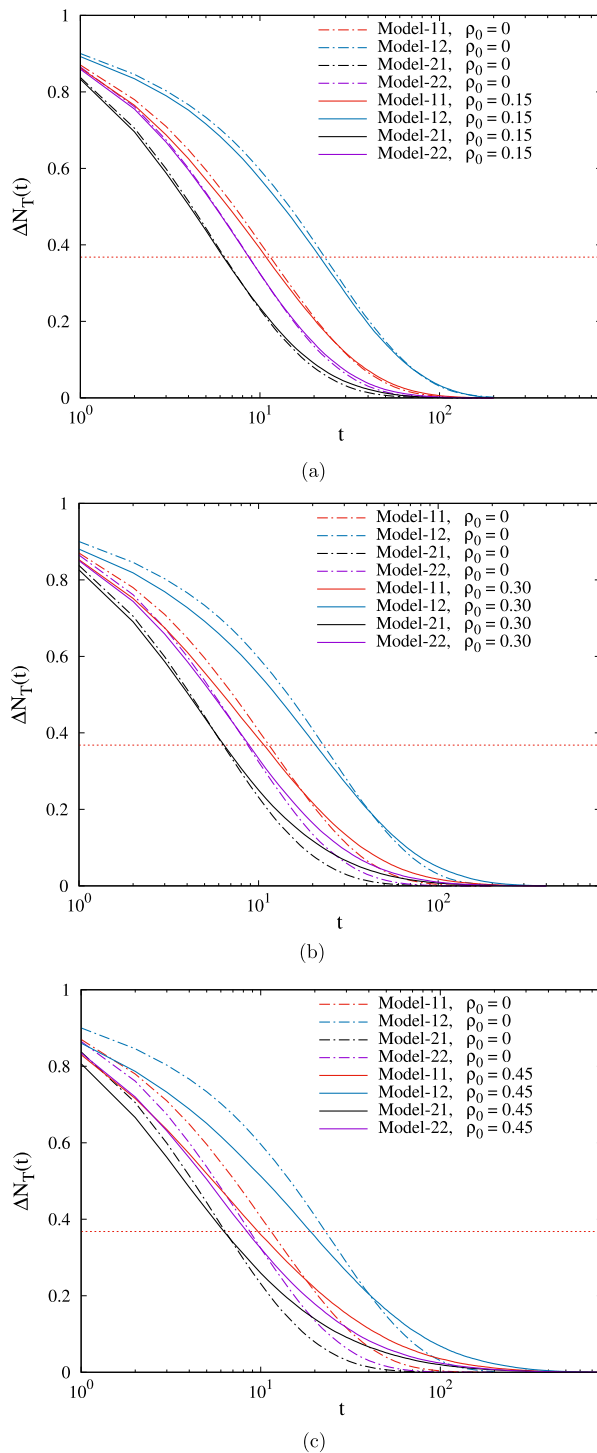
Fig. 13. Temporal behavior of the normalized deviation $\Delta N_T(t)$ (Eq. (3)) for the four models (Model-ij, $i, j = 1, 2$) created by combining the two types of chasers and targets, as shown in Table 3. The solid lines represent the results obtained in the presence of obstacles C_2 (see, Table 2) at densities $\rho_0 = 0.15$(a), 0.30(b), 0.45(c). The dashed lines represent the temporal behavior of $\Delta N_T(t)$ in the absence of obstacles. Other parameters: $L = 128$, $N_0^C/N_0^T = 720/800 = 0.9$.

$\rho_0 = 0 - 0.45$. At first, we present the results of simulations for one representative linear segment, i.e., for the trimer (A_3) at densities $\rho_0 = 0.15, \ 0.30, \ 0.45$. The corresponding time dependences of the normalized deviation $\Delta N_T(t)$ (see,

Table 1
Jamming coverages $\rho_J^{(x)}$ for various k-mers (x) of length $\ell^{(x)}$ on a square lattice. The estimated statistical errors are on the last given digits.

(x)	k-mer	$\ell^{(x)}$	$\rho_J^{(x)}$
(A_1)	•	0	1.0
(A_2)	●—●	1	0.9067
(A_3)	●—•—●	2	0.8465
(A_4)	●—•—•—●	3	0.8102
(A_5)	●—•—•—•—●	4	0.7867
(A_6)	●—•—•—•—•—●	5	0.7699
(A_7)	●—•—•—•—•—•—●	6	0.7578

Table 2
Jamming coverages $\rho_J^{(x)}$ for extended shapes (x) of size $s^{(x)}$ on a square lattice. The estimated statistical errors are on the last given digits.

(x)	Shape	$s^{(x)}$	$\rho_J^{(x)}$
(C_1)		2	0.6988
(C_2)		4	0.5691

Table 3
Four models created by combining the two types of chasers and targets. Depending on the sighting range σ, chasers and targets with different chasing and avoidance skills, respectively, can be distinguished.

Model	Chaser	Target
Model-11	Chaser-I ($\sigma = 1$)	Target-I ($\sigma = 1$)
Model-12	Chaser-I ($\sigma = 1$)	Target-II ($\sigma = 2$)
Model-21	Chaser-II ($\sigma = 2$)	Target-I ($\sigma = 1$)
Model-22	Chaser-II ($\sigma = 2$)	Target-II ($\sigma = 2$)

Eq. (3)) for the aforementioned densities ρ_0 are given in Fig. 11 together with the result obtained in the absence of the obstacles. It can be seen that the capture dynamics gets slower, and the evolution of the number of targets $N_T(t)$ toward the asymptotic value $N_T(\infty)$ takes place on much wider time scale when the density of trimers ρ_0 increases. We note that different choices of the linear segments give qualitatively similar results.

In Fig. 12 we compare the temporal evolution of the normalized deviation $\Delta N_T(t)$ (see, Eq. (3)) for the linear segments (k-mers) covering $k = 1, 2, \ldots, 7$ lattice sites. Time dependences of $\Delta N_T(t)$ are displayed both for the density $\rho_0 = 0.30$ of obstacles, and for the case of lattice without obstacles. In the presence of k-mers, reduction in the number of targets $N_T(t)$ takes place on the approximately equal time scale for all k-mers. As expected, the decrease of the number of targets $N_T(t)$ with time is significantly faster in the absence of obstacles. It is interesting that $\Delta N_T(t)$ vs. t curves have similar shapes for all finite-size k-mers ($k > 1$). As can be seen, for the point-like obstacles ($k = 1$) the capture dynamics gets slower, especially in the intermediate time regime. There is an important difference between the deposition of point-like and elongated obstacles on a square lattice. Deposition of elongated objects is characterized with domains of parallel objects and large areas of unoccupied sites. Blocking of the lattice area is enhanced with the growth of the obstacle length, making the surface more porous (unoccupied sites can form open and large pores). On the other hand, the point-like objects (monomers) cover the surface more uniformly and efficiently. Lower porosity of the surface is responsible for the reduced mobility of species, and therefore for slower dynamics in the case of the point-like obstacles.

In Section 2 we have introduced the chasers and the targets with different chasing and avoidance skills, respectively. Depending on the sighting range σ, less ($\sigma = 1$) and more ($\sigma = 2$) capable chasers or targets can be distinguished (see, Table 3). It is now useful to explore the relationship between the ability of species and the capture dynamics. In Fig. 13 we compare the temporal evolution of the normalized deviation $\Delta N_T(t)$ (see, Eq. (3)) for all four combinations of previously defined species, as shown in Table 3. The results are given for the obstacle C_2 (see, Table 2) at densities $\rho_0 = 0.15, 0.30, 0.45$, as well as for the lattice without obstacles. By comparing the results for the Model-12 with those for the Model-22 and Model-11, it can be observed that the less capable chasers or the more capable targets cause a significantly slower decrease in the number of targets $N_T(t)$ to the asymptotic value $N_T(\infty)$. On the contrary, by comparing results for the Model-21 with those for the Model-22 and Model-11, it is obvious that the less capable targets or the more capable chasers hasten the dynamics of the chasing process.

As can be seen from Fig. 13 the decrease in the number of targets in the presence of obstacles at sufficiently small times is faster than in the absence of obstacles, and this effect is more pronounced for the larger densities of obstacles.

At the beginning of the process, the density of targets is high, so that the mean distance between them is small. As a consequence, a chaser quickly and efficiently find targets in its own vicinity. At the same time, the obstacles make it difficult for the targets to escape from the nearest chaser. Therefore, the presence of obstacles increases the efficiency of chasers in the initial phase of the evolution of the number of targets.

However, in the late chasing stage inversion occurs, i.e., the presence of obstacles slows down the dynamics of the system (see, Fig. 13). Indeed, the lower is the concentration of the targets, the longer is the time necessary for the chaser to find a target and catch it. Thus, the mean distance that a chaser crosses between two consecutive catches increases over time. Along the longer path, chaser will interact with a larger number of obstacles. Therefore, obstacles more effectively hinder the chasers when the density of the targets becomes small enough.

In models with more capable chasers (Model-22 and Model-21), the presence of obstacles induces larger changes in the dynamics of the system in the late chasing stage than in the initial phase of the process. At the beginning of the process, more capable chasers quickly and efficiently find the neighboring targets, regardless of whether there are obstacles or not. However, less capable chasers interact with a larger number of obstacles between two consecutive catches. Consequently, in the cases of less capable chasers (Model-11 and Model-12), the differences in the dynamics of the system with and without obstacles are pronounced even in the initial phase of the evolution of the number of targets.

4. Summary

We have numerically studied a stochastic lattice model describing a group chase and escape with sight-limited chasers and targets. We take into account the spatial structure of the environment where the species coexist in an explicit way. The environment heterogeneities are built by randomly selecting a fraction of the sites of the square lattice that are considered forbidden for the species. Specifically, the obstacles are represented by non-overlapping lattice shapes that are randomly placed and fixed on the lattice. Our focus in this paper was to investigate the role that density and shape of obstacles plays in the time evolution of the number of targets, $N_T(t)$. Basic mechanisms responsible for the studied phenomenon were investigated and for this reason we ignored the birth/death processes. Such processes will be considered in the future work.

It was shown that the stretched exponential behavior (Eq. (1)) excellently describes the temporal dependence of the number of targets $N_T(t)$ regardless of whether the obstacles are present or not. The characteristic timescale τ was found to decrease with the initial density of targets ρ_0^T according to a power-law (2), $\tau \propto (\rho_0^T)^{-\gamma}$. Furthermore, it was obtained that the characteristic time τ increases with the density of obstacles ρ_0. This effect was much more pronounced at the lower densities ρ_0 investigated.

We have considered the behavior of the stretched exponent β (Eq. (1)) as a function of the initial density of targets ρ_0^T and the density of obstacles ρ_0. At the given density of obstacles ρ_0, the exponent β is weakly dependent on the initial density of targets ρ_0^T, provided the initial ratio of chasers to targets $N_0^C/N_0^T = \rho_0^C/\rho_0^T$ is constant. However, the stretching exponent β, which measures the rate of the chasing process, decreases with the density of the obstacles ρ_0. At the fixed density ρ_0, parameter β depends on the shape and size of the obstacles.

The simulations have shown that the time dependences of $\Delta N_T(t)$ (Eq. (3)), at the fixed density ρ_0, are very similar for all finite-size k-mers ($k > 1$). However, slowing down in the capture dynamics was observed in the case of the point-like obstacles ($k = 1$). Indeed, randomly deposited monomers cover the lattice more uniformly and therefore efficiently reduce the mobility of species.

We have discussed the significance of the sighting range σ of species for governing the capture dynamics in the presence of obstacles. It was shown that the less capable chasers/targets ($\sigma = 1$) or the more capable targets/chasers ($\sigma = 2$) slow-down/hasten the dynamics of the chasing process. It was observed that the decrease in the number of targets in the presence of obstacles at sufficiently small/large times is faster/slower than in the absence of obstacles, and this effect is more pronounced for larger densities of obstacles. In the case of more capable chasers ($\sigma = 2$), the presence of obstacles induces larger changes in the dynamics of the system in the late chasing stage than in the initial phase of the process. In the case of the less capable chasers ($\sigma = 1$), differences in the dynamics of the system with and without obstacles are pronounced in the initial phase of the evolution of the number of targets.

This model can easily be generalized using obstacles of various shapes, describing the system of interest. Features of the chasers and escapees as well as their capabilities can also be modified according to the system of interest. Our simulation can describe in a simple manner some real life systems or tools that are still in development, and becoming more important. Application can be seen even in robotics, especially in unmanned vehicles, designed to avoid obstacles (something that could be developed in new versions of our simulation) and win certain targets that are fixed or in motion, depending on its goal. For instance, one can observe a security robot trying to capture and eliminate malicious evader that is trying to escape. Robot can be instructed not to capture but to follow and monitor the evader (something that could also be developed in other versions of the simulation) and report its behavior. Just visual monitoring can be greatly useful in the home caring situations, for example following elderly people and report if there is an emergency.

Acknowledgments

References

[1] A. Czirók, E. Ben-Jacob, I. Cohen, T. Vicsek, Formation of complex bacterial colonies via self-generated vortices, Phys. Rev. E 54 (1996) 1791–1801.

[2] A. Czirók, M. Matsushita, T. Vicsek, Theory of periodic swarming of bacteria: Application to proteus mirabilis, Phys. Rev. E 63 (2001) 031915.

[3] A. Sokolov, I.S. Aranson, J.O. Kessler, R.E. Goldstein, Concentration dependence of the collective dynamics of swimming bacteria, Phys. Rev. Lett. 98 (2007) 158102.

[4] D.A. Kessler, H. Levine, Pattern formation in dictyostelium via the dynamics of cooperative biological entities, Phys. Rev. E 48 (1993) 4801–4804.

[5] S. Nagano, Diffusion-assisted aggregation and synchronization in dictyostelium discoideum, Phys. Rev. Lett. 80 (1998) 4826–4829.

[6] W.-J. Rappel, A. Nicol, A. Sarkissian, H. Levine, W.F. Loomis, Self-organized vortex state in two-dimensional dictyostelium dynamics, Phys. Rev. Lett. 83 (1999) 1247–1250.

[7] B. Szabó, G.J. Szöllösi, B. Gönci, Z. Jurányi, D. Selmeczi, T. Vicsek, Phase transition in the collective migration of tissue cells: Experiment and model, Phys. Rev. E 74 (2006) 061908.

[8] P. Friedl, D. Gilmour, Collective cell migration in morphogenesis, regeneration and cancer, Nat. Rev. Mol. Cell Biol. 10 (2009) 445457.

[9] J.M. Belmonte, G.L. Thomas, L.G. Brunnet, R.M.C. de Almeida, H. Chaté, Selfpropelled particle model for cell-sorting phenomena, Phys. Rev. Lett. 100 (2008) 248702.

[10] J. Buhl, D.J.T. Sumpter, I.D. Couzin, J.J. Hale, E. Despland, E.R. Miller, S.J. Simpson, From disorder to order in marching locusts, Science 312 (2006) 1402–1406.

[11] B. Collignon, J.L. Deneubourg, C. Detrain, Leader-based and self-organized communication: Modelling group-mass recruitment in ants, J. Theoret. Biol. 313 (2012) 79–86.

[12] C. Becco, N. Vandewalle, J. Delcourt, P. Poncin, Experimental evidences of a structural and dynamical transition in fish school, Physica A 367 (2006) 487–493.

[13] M. Zheng, Y. Kashimori, O. Hoshino, K. Fujita, T. Kambara, Behavior pattern (innate action) of individuals in fish schools generating efficient collective evasion from predation, J. Theoret. Biol. 235 (2005) 153–167.

[14] I.L. Bajec, F.H. Heppner, Organized flight in birds, Anim. Behav. 78 (2009) 777–789.

[15] C.K. Hemelrijk, H. Hildenbrandt, Some causes of the variable shape of flocks of birds, PLoS One 6 (2011) e22479.

[16] D. Helbing, F. Schweitzer, J. Keltsch, P. Molnár, Active walker model for the formation of human and animal trail systems, Phys. Rev. E 56 (1997) 2527–2539.

[17] D. Helbing, I. Farkas, T. Vicsek, Simulating dynamical features of escape panic, Nature 407 (2000) 487–490.

[18] M. Moussaïd, D. Helbing, G. Theraulaz, How simple rules determine pedestrian behavior and crowd disasters, Proc. Natl. Acad. Sci. 108 (2011) 6884–6888.

[19] J. Kwak, H.-H. Jo, T. Luttinen, I. Kosonen, Collective dynamics of pedestrians interacting with attractions, Phys. Rev. E 88 (2013) 062810.

[20] M. Gutiérrez-Roig, O. Sagarra, A. Oltra, J.R.B. Palmer, F. Bartumeus, A. Díaz-Guilera, J. Perelló, Active and reactive behaviour in human mobility: The influence of attraction points on pedestrians, Open Sci. 3 (2016).

[21] T. Vicsek, A. Zafeiris, Collective motion, Phys. Rep. 517 (2012) 71–140.

[22] P.J. Nahin, Chases and Escapes: The Mathematics of Pursuit and Evasion, Princeton University Press, Princeton, NJ, 2007.

[23] P.L. Krapivsky, S. Redner, Kinetics of a diffusive capture process: Lamb besieged by a pride of lions, J. Phys. A: Math. Gen. 29 (1996) 5347.

[24] G. Oshanin, O. Vasilyev, P.L. Krapivsky, J. Klafter, Survival of an evasive prey, Proc. Natl. Acad. Sci. 106 (2009) 13696–13701.

[25] R. Escobedo, C. Muro, L. Spector, R.P. Coppinger, Group size, individual role differentiation and effectiveness of cooperation in a homogeneous group of hunters, J. R. Soc. Interface 11 (2014) http://dx.doi.org/10.1098/rsif.2014.0204.

[26] A. Kamimura, T. Ohira, Group chase and escape, New J. Phys. 12 (2010) 053013.

[27] T. Vicsek, Nature 466 (2010) 43.

[28] R. Nishi, A. Kamimura, K. Nishinari, T. Ohira, Group chase and escape with conversion from targets to chasers, Physica A 391 (2012) 337–342.

[29] P. Romanczuk, I.D. Couzin, L. Schimansky-Geier, Collective motion due to individual escape and pursuit response, Phys. Rev. Lett. 102 (2009) 010602.

[30] V. Zhdankin, J.C. Sprott, Simple predator-prey swarming model, Phys. Rev. E 82 (2010) 056209.

[31] X.-P. Han, T. Zhou, B.-H. Wang, Scaling mobility patterns and collective movements: Deterministic walks in lattices, Phys. Rev. E 83 (2011) 056108.

[32] T.H. Chung, G.A. Hollinger, V. Isler, Search and pursuit-evasion in mobile robotics, Auton. Robots 31 (2011) 299.

[33] T. Iwama, M. Sato, Group chase and escape with some fast chasers, Phys. Rev. E 86 (2012) 067102.

[34] S. Yang, S. Jiang, L. Jiang, G. Li, Z. Han, Aggregation increases prey survival time in group chase and escape, New J. Phys. 16 (2014) 083006.

[35] Y. Chen, T. Kolokolnikov, A minimal model of predators–warm interactions, J. R. Soc. Interface 11 (2014) http://dx.doi.org/10.1098/rsif.2013.1208.

[36] A. Kamimura, S. Matsumoto, T. Nogawa, N. Ito, T. Ohira, Stochastic resonance with group chase and escape, in: 2011 21st International Conference on Noise and Fluctuations, 2011, pp. 200–203.

[37] J.W. Evans, Random and cooperative sequential adsorption, Rev. Modern Phys. 65 (1993) 1281–1329.

[38] Lj Budinski-Petković, I. Lončarević, D. Dujak, A. Karač, J.R. Šćepanović, Z.M. Jakšić, S.B. Vrhovac, Particle morphology effects in random sequential adsorption, Phys. Rev. E 95 (2017) 022114.

[39] N. Boccara, O. Roblin, M. Roger, Automata network predator-prey model with pursuit and evasion, Phys. Rev. E 50 (1994) 4531–4541.

[40] A.F. Rozenfeld, E.V. Albano, Critical and oscillatory behavior of a system of smart preys and predators, Phys. Rev. E 63 (2001) 061907.

[41] H. Chaté, F. Ginelli, G. Grégoire, F. Raynaud, Collective motion of self-propelled particles interacting without cohesion, Phys. Rev. E 77 (2008) 046113.

[42] L. Angelani, Collective predation and escape strategies, Phys. Rev. Lett. 109 (2012) 118104.

[43] T. Vicsek, A. Czirók, E. Ben-Jacob, I. Cohen, O. Shochet, Novel type of phase transition in a system of self-driven particles, Phys. Rev. Lett. 75 (1995) 1226–1229.

[44] H. Wang, W. Han, J. Yang, Group chase and escape with sight-limited chasers, Physica A 465 (2017) 34–39.

[45] J. Travis, Do wandering albatrosses care about math? Science 318 (2007) 742–743.

[46] N. Vandewalle, S. Galam, M. Kramer, A new universality for random sequential deposition of needles, Eur. Phys. J. B 14 (2000) 407–410.

[47] V. Cornette, A.J. Ramirez-Pastor, F. Nieto, Percolation of polyatomic species on a square lattice, Eur. Phys. J. B 36 (2003) 391–399.

[48] M. Bruna, S.J. Chapman, Diffusion of multiple species with excluded-volume effects, J. Chem. Phys. 137 (2012) 204116.

[49] M. Schwarzl, A. Godec, G. Oshanin, R. Metzler, A single predator charging a herd of prey: Effects of self volume and predator–prey decision-making, J. Phys. A 49 (2016) 225601.

[50] R. Hilfer, Analytical representations for relaxation functions of glasses, J. Non-Cryst. Solids 305 (2002) 122–126.

[51] Lj. Budinski-Petković, I. Lončarević, Z.M. Jakšić, S.B. Vrhovac, N.M. Švrakić, Simulation study of anisotropic random sequential adsorption of extended objects on a triangular lattice, Phys. Rev. E 84 (2011) 051601.